DYNAMIC MODELING AND SIMULATION OF A CABLE/TOW BODY SYSTEM OF A HELICOPTER

J.V.R. Prasad, Zhenhao Jing, Lakshmi Sankar
School of Aerospace Engineering
Georgia Institute of Technology
Atlanta, GA 30332, USA

Chengjian He, Jan Goericke
Advanced Rotorcraft Technology, Inc.
Sunnyvale, CA 94085
USA

Abstract

For cases involving a helicopter involving a towing cable with an end mass, when the mass of the towed body is of the same order of magnitude of the towing cable mass, the dynamic analysis and simulation of the resulting system can become quite challenging, especially in cases that involve large cable lengths. This paper develops an approach utilizing the natural modes of a hanging string with tip mass in free vibration. With a modal representation of the cable deflection, the problem solution reduces to response to applied aerodynamic forces on the cable and the towed body. The aerodynamic forces acting on the cable are calculated using the cross-flow principle and the aerodynamic forces on the towed body are included using a table look up variations with angle of attack and sideslip angles, which are pre-computed using a comprehensive CFD analysis. The resulting equations of motion in generalized coordinates are numerically integrated for determining the cable transient deflections due to helicopter maneuvers. Results from transient simulation of the cable/tow body system for selected cases of helicopter maneuvers are presented. Further, the impact of variations of cable/tow body system parameters on the tow body transient motion are analyzed.

1. NOMENCLATURE

g	Constant of acceleration due to gravity
s	Lagrangian coordinate that traces the cable from tow body to helicopter
x, y, z	Longitudinal, lateral and vertical axes with origin at the cable attachment point of the helicopter
u, v, w	Longitudinal, lateral and vertical deflections of an arbitrary point of cable
ρ	Cable mass per unit length
T	Cable Tension
F_{aero}	Cable aerodynamic force
$\hat{e}_{aero}$	Direction of cable aerodynamic force
α	Cable angle of attack
q_i, M_i, Q_i	Generalized coordinate, generalized mass and generalized force
J_0, Y_0	Bessel functions of first and second kind of order zero
μ	Ratio of tow body mass to cable mass

2. INTRODUCTION

Modeling and analysis of a helicopter with an external load connected by a cable or towing of a body using a cable has been extensively studied in the literature[1, 2]. Most of those studies involved the mass of the slung load/ tow body being an order of magnitude larger than that of the cable. When the mass of the load/tow body is of the same order of magnitude of the cable mass, the dynamic analysis and simulation of the resulting system can become quite challenging, especially in cases that involve large cable lengths, as aerodynamic forces on the cable, which often are neglected, become that much more important.

Previous efforts[3, 4] have utilized a discretized model, wherein the cable is discretized into multiple segments with each segment modeled as a three-degree-of-freedom system in space, and joining them with proper tension forces and kinematic

Presented at 45th European Rotorcraft Forum, Warsaw, Poland, 17-20 September, 2019
NAVAIR Public Release 2019-571. Distribution Statement A – “Approved for public release; distribution is unlimited”

constraints. With such a discretized model, one can obtain solution of the cable deflection under steady state conditions of helicopter motion. But for cable transient motion arising from helicopter accelerations / deceleration or from effects due to external gusts, the tension forces at some segments may become close to zero due to the light weight of the attached load. This can lead to a stiff system of equations, requiring very small integration step size in order to maintain fidelity of the numerical simulation, thus posing an issue for real time simulations without a compromise on solution fidelity.

This paper develops an alternate approach, which utilizes the natural modes of a hanging string with tip mass in free vibration[5]. The external aerodynamic forces are applied to the modal equations using the generalized force formulation, and the simulation output is the superposition of the mode shapes multiplied by the corresponding generalized coordinates.

With a modal representation of the cable deflections, the problem solution reduces to response to applied aerodynamic forces on the cable and the end mass (tow body). The aerodynamic forces acting on the cable are calculated using the cross-flow principle[6] and the aerodynamic forces on the end mass body are obtained using a pre-computed table look up variations with angle of attack and sideslip angles.

The paper is organized as follows: First, the governing equation of the entire cable/tow body system are derived. Next, the free vibration mode shapes and modal frequencies of a cable with end mass (towed body) are computed and are compared with known test cases. This is followed by presentation of results from transient simulations of the cable/tow body system for selected cases of helicopter maneuvers. Next, the impact of variations of cable/tow body system parameters on the transient motion of the towed body are analyzed. Finally, conclusions are drawn based on the presented results, followed by recommendations for future work.

3. TOWING CABLE DYNAMICS MODELING

The approach pursued in this paper for modeling the towing cable dynamics is to use a modal approximation in order to reduce the degrees of freedom and, hence, the computational cost associated with integration of the resulting equations. To this end, (1) the governing equation of the entire cable is derived, (2) its mode shapes and modal frequencies are determined and compared with known test cases, and (3) the towing cable dynamic equations are obtained in terms of the generalized coordinates.

3.1. Derivation of Governing Equations for the Towing Cable

To derive the governing equation for the towing cable, a coordinate, s, is defined which traces the cable from the bottom towed body to the towing aircraft as shown in Fig. 1. The longitudinal, lateral, and vertical deflections, u, v, w as well as the cable coordinate, s, are noted in the illustration.

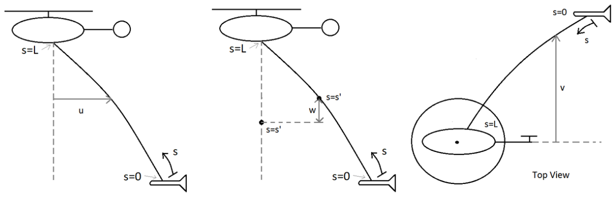

Figure 1. Towing cable configuration and definition of important parameters.

For an arbitrary infinitesimally small segment, the forces acting on a cable segment are defined as shown in Fig. 2 with the cable mass per unit length, ρ, the cable coordinate, s, the cable tension vector, T, and the cable aerodynamic force, F_{aero}.

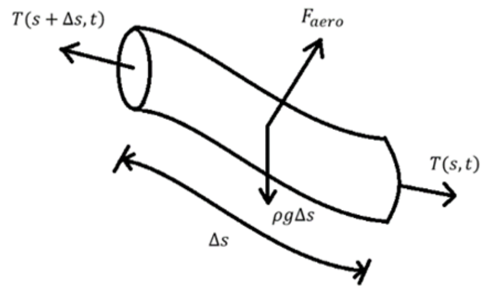

Figure 2. Definition of important parameters for the towing cable segment.

Considering the longitudinal cable deflection exclusively and starting from Newton's Second Law,

(1) $$m\vec{a} = \sum \vec{F}$$

Presented at 45th European Rotorcraft Forum, Warsaw, Poland, 17-20 September, 2019
NAVAIR Public Release 2019-571. Distribution Statement A – "Approved for public release; distribution is unlimited"

An application of Eq. 1 to the cable segment leads to

$$(2) \quad \rho\Delta s \frac{\partial^2 u(s,t)}{\partial t^2} = -T_x(s,t) + T_x(s+\Delta s,t) + F_{x_{aero}}$$

with the longitudinal deflection, u, and the longitudinal components of tension force T_x and aerodynamic force $F_{x\,aero}$. Dividing both sides of Eq. 2 by Δs and with $\Delta s \rightarrow 0$, the equation becomes

$$(3) \quad \rho \frac{\partial^2 u}{\partial t^2} = \frac{\partial T_x(s,t)}{\partial s} + \frac{\partial F_{x\,aero}}{\partial s}$$

The cable longitudinal tension force, $T_x(s,t)$, can be expressed as

$$(4) \quad T_x(s,t) = \left\|\vec{T}(s,t)\right\| \frac{\frac{\partial u}{\partial s}}{\sqrt{\left(\frac{\partial u}{\partial s}\right)^2 + \left(\frac{\partial v}{\partial s}\right)^2 + \left(1-\frac{\partial w}{\partial s}\right)^2}}$$

For the case of an inextensible cable, $\sqrt{\left(\frac{\partial u}{\partial s}\right)^2 + \left(\frac{\partial v}{\partial s}\right)^2 + \left(1-\frac{\partial w}{\partial s}\right)^2} = 1$. Hence, for the Inextensible cable and with the cable mass per unit length, , Eq. 3 can be written as

$$(5) \quad \rho \frac{\partial^2 u}{\partial t^2} = \frac{\partial}{\partial s}\left(\left\|\vec{T}\right\| \frac{\partial u}{\partial s}\right) + \frac{\partial F_{x\,aero}}{\partial s}$$

The aerodynamic force, $F_{x\,aero}$, acting on the towing cable is calculated using the Cross Flow Principle6, which states that, for towing cables with circular cross-section, the aerodynamic force direction is perpendicular to the cable tangential direction and is always in the plane defined by the free-stream direction and the cable tangential direction. The equation for the aerodynamic force along the cable coordinate s and at time t is given as

$$(6) \quad \vec{F}_{aero}(s,t) = C_D q_{dynpr} S_{ref} (\sin(\alpha))^2 \hat{e}_{aero}$$

with the drag coefficient C_D, the dynamic pressure $q_{dynpr} = \frac{1}{2}\rho_\infty\left(\left(V_\infty + \frac{\partial u}{\partial t}\right)^2 + \left(\frac{\partial v}{\partial t}\right)^2 + \left(\frac{\partial w}{\partial t}\right)^2\right)$, free stream air density ρ_∞, cable reference area $S_{ref} = d\Delta s$, and the cable diameter, d. The angle of attack, α, is calculated as

$$(7) \quad \alpha = \cos^{-1}\left(\frac{\|\vec{W}\cdot\vec{U}\|}{\|\vec{W}\|\cdot\|\vec{U}\|}\right)$$

with the local tangential vector, $\vec{W} = \frac{\partial u}{\partial s}\hat{\imath} + \frac{\partial v}{\partial s}\hat{\jmath} + (1-\frac{\partial w}{\partial s})\hat{k}$, and the cable velocity vector, $\vec{U} = (V_\infty + \frac{\partial u}{\partial t})\hat{\imath} + \frac{\partial v}{\partial t}\hat{\jmath} + \frac{\partial w}{\partial t}\hat{k}$. The direction of the aerodynamic force is calculated as

$$(8) \quad \hat{e}_{aero} = \frac{(\vec{U}\times\vec{W})\times\vec{W}}{\|(\vec{U}\times\vec{W})\times\vec{W}\|}$$

The aerodynamic force component along the cable (i.e., longitudinally in the x-direction) is calculated as

$$(9) \quad F_{x\,aero} = \vec{F}_{aero} \cdot \begin{bmatrix}1\\0\\0\end{bmatrix}$$

The cable tension force, $\left\|\vec{T}(s,t)\right\|$, at any point along the cable consists of the summation of all cable forces below the point of interest including the aerodynamic and inertial forces acting on the tow cable and the towed body. In order to reduce the computational complexity, the free vibration mode shapes of the cable are obtained first and then are used to compute the generalized forces for the cable/tow body system as shown in the next sub-section.

3.2. Determination of Free Vibration Mode Shapes and Modal Frequencies

Assumption: The cable mode shapes and modal frequencies depend on the cable tension, $\left\|\vec{T}(s,t)\right\|$. The formulation for the cable tension that considers the towed body and cable aerodynamics is highly nonlinear which makes finding the cable mode shapes and frequencies unnecessarily complicated. Hence, the aerodynamic forces of the towing cable and the towed body are neglected when finding the mode shapes and modal frequencies of the towing cable. Thus, the free vibratory dynamics of a hanging cable with a point mass are represented. The dynamic equation of the towing cable without aerodynamics can be derived from Eq. 5 as

$$(10) \quad \rho \frac{\partial^2 u}{\partial t^2} = \frac{\partial}{\partial s}\left(\left\|\vec{T}\right\| \frac{\partial u}{\partial s}\right)$$

where the magnitude of the tension force can be approximated as

$$(11) \quad \left\|\vec{T}\right\| \approx m_{TB}g + \rho g s = F_1 + F_2 s$$

with the towed body mass, m_{TB}, the cable mass per unit length, ρ, the gravitational constant, g, and the cable coordinate, s. Assuming a solution of the form, $u = \bar{u}(s)\cdot e^{i\omega t}$, and dividing both sides of Eq. 10 by $\rho\omega^2$ results in

Presented at 45th European Rotorcraft Forum, Warsaw, Poland, 17-20 September, 2019
NAVAIR Public Release 2019-571. Distribution Statement A – “Approved for public release; distribution is unlimited”

(12) $$\frac{\partial}{\partial s}\left(\frac{\|\vec{T}\|}{\rho\omega^2}\frac{\partial \bar{u}}{\partial s}\right)+\bar{u}=0$$

In order to obtain an analytical solution to Eq. 12, Sujith and Hodges[5] use a change of variable with the new variable, η, defined as

(13) $$\eta=\frac{2\sqrt{\rho}\cdot\omega\cdot\sqrt{\|\vec{T}\|}}{\|\vec{T}\|'}$$

where $\|\vec{T}\|'=\frac{\partial(\|\vec{T}\|)}{\partial s}$. For the case of dynamics in vacuum, i.e., no aerodynamics, $\|\vec{T}\|=F_1+F_2 s$, which results in $\|\vec{T}\|'=F_2=constant$. Consequently, Eq. 13 becomes

(14) $$\frac{\partial\eta}{\partial s}=\frac{2\sqrt{\rho}\cdot\omega\cdot\frac{1}{2}\|\vec{T}\|'}{\sqrt{\|\vec{T}\|\|\vec{T}\|'}}=\frac{\omega\sqrt{\rho}}{\sqrt{\|\vec{T}\|}} \text{ and } \left(\frac{\partial\eta}{\partial s}\right)^2=\frac{\omega^2\rho}{\|\vec{T}\|}$$

Substituting the new variable η, Eq. 12 becomes

(15) $$\frac{\partial}{\partial s}\left(\left(\frac{\partial s}{\partial\eta}\right)^2\frac{\partial\bar{u}}{\partial s}\right)+\bar{u}=0$$

After expanding the squared term and rearranging for the new variable, η , the governing Eq. 12 becomes

(16) $$\frac{\partial^2\bar{u}}{\partial\eta^2}+\frac{1}{\eta}\frac{\partial\bar{u}}{\partial\eta}+\bar{u}=0$$

Equation 16 is in the form of a Bessel's equation with a solution of Bessel functions of order zero, $J_0(\eta)$ and $Y_0(\eta)$. The general solution can be written as

(17) $$\bar{u}=C_1\cdot J_0(\eta)+C_2\cdot Y_0(\eta)$$

Boundary Conditions: Recall that the new variable, η, is a function of s, *i.e.*, $\eta(s)$. For convenience, define $\eta(0)=\eta_0$ (cable end at towed body) and $\eta(L)=\eta_L$ (cable attachment end with cable length, L). The boundary condition at the cable attachment point to the towing aircraft, i.e., at $s=L$, is

(18) $$\bar{u}(\eta_L)=C_1\cdot J_0(\eta_L)+C_2\cdot Y_0(\eta_L)=0$$

with non-trivial solution as $C_1=-Y_0(\eta_L)\ and\ C_2=J_0(\eta_L)$.

The boundary condition at the cable attachment point to the towed body, $s=0$, with the towed body mass, m_{TB}, is

(19) $$m_{TB}\frac{\partial^2 u(0,t)}{\partial t^2}=\|\vec{T}(0,t)\|\cdot\frac{\partial u(0,t)}{\partial s}$$

Using $u=\bar{u}(s)\cdot e^{i\omega t}$ and after some rearranging, the equation for the boundary condition at $s=0$ becomes

(20) $$\sqrt{\rho F_1}\frac{\partial(C_1\cdot J_0(\eta_0)+C_2\cdot Y_0(\eta_0))}{\partial\eta}+m_{TB}\cdot(C_1\cdot J_0(\eta_0)+C_2\cdot Y_0(\eta_0))\cdot\omega=0$$

Using the relationships that $\frac{\partial J_0(z)}{\partial z}=-J_1(z)$; $\frac{\partial Y_0(z)}{\partial z}=-Y_1(z)$ with J_1 and Y_1 being Bessel functions of order 1, and after substituting C_1 and C_2 as obtained from the boundary condition at s = L, one obtains

(21) $$\sqrt{\rho F_1}[Y_0(\eta_L)J_1(\eta_0)-J_0(\eta_L)Y_1(\eta_0)]+m\omega\cdot[-Y_0(\eta_L)\cdot J_0(\eta_0)+J_0(\eta_L)\cdot Y_0(\eta_0)]=0$$

where $\eta=\frac{2\sqrt{\rho}\cdot\omega\cdot\sqrt{\|T\|}}{\|T\|'}$, $\|T\|=F_1+F_2 s$, $\eta_0=\frac{2\sqrt{\rho}\cdot\omega\cdot\sqrt{F_1}}{F_2}$, and $\eta_L=\frac{2\sqrt{\rho}\cdot\omega\cdot\sqrt{F_1+F_2 L}}{F_2}$.

Equation 21 is the characteristic equation of the towed body system, which determines the fundamental frequencies of free vibration of the system. Once the modal frequencies are determined using Eq. 21, the corresponding free vibration mode shapes are calculated using

(22) $$\bar{u}_i=-Y_0(\eta_L)\cdot J_0(\eta(\omega_i,s))+J_0(\eta_L)\cdot Y_0(\eta(\omega_i,s))$$

Example estimates of the modal frequencies and corresponding mode shapes are shown in Fig. 3. Note that for a cable without tip mass and with a rigid link pendulum of length L = 20 m, the theoretical pendulum frequency is $=\sqrt{\frac{g}{L}}$ rad/s. As the mass ratio between cable and towed body increases, the first mode of the towing cable behaves close to a theoretical rigid pendulum, as seen from the value of the first modal frequency for the case of a 999 kg tip mass (Fig. 3(d)). For the same 999 kg tip mass, the cable mode shapes are similar to the results for a cable that is fixed at both ends.

Presented at 45th European Rotorcraft Forum, Warsaw, Poland, 17-20 September, 2019

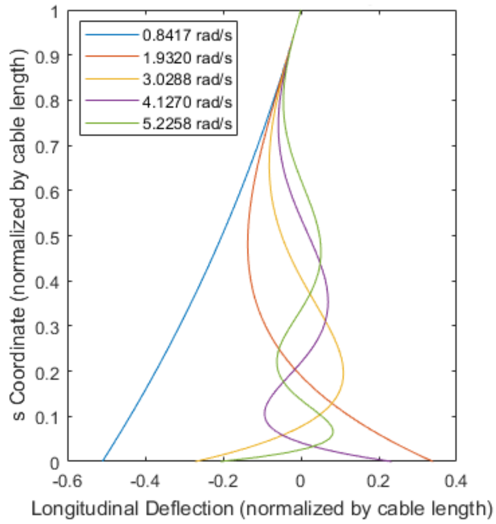

(a) $m_{TB} = 0, L = 20\ m$

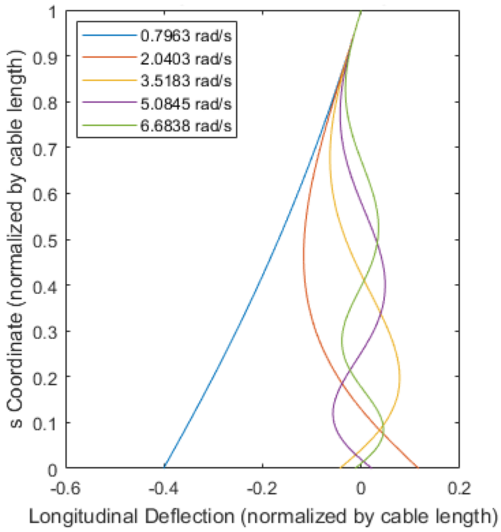

(b) $m_{TB} = 0.1\ kg, L = 20\ m$

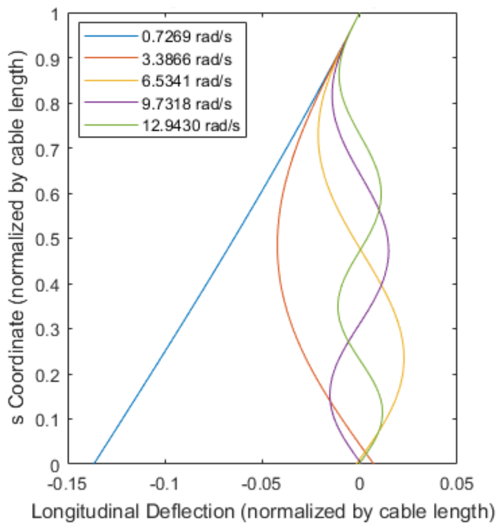

(c) $m_{TB} = 1\ kg, L = 20\ m$

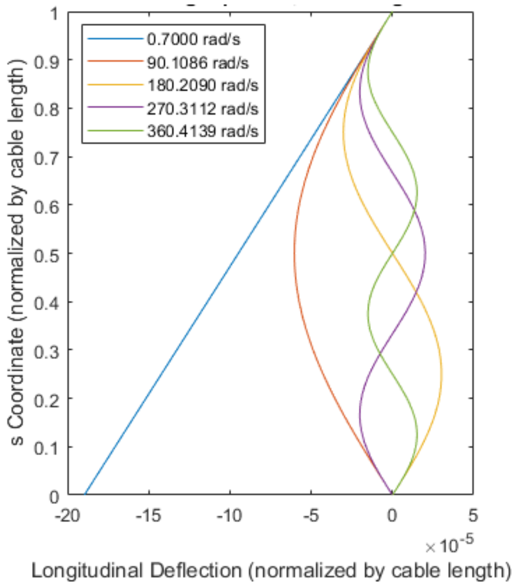

(d) $m_{TB} = 999\ kg, L = 20\ m$

Figure 3. Examples of mode shapes and modal frequencies for different cases of ratio of tow body mass to cable mass with cable length L = 20 m, and cable mass per unit length $\rho = 0.02976\ \mathrm{kg/m}$.

3.3. Generalized Equations of Motion with Aerodynamic Forces

The response of the towed body system governed by the generalized equation of motion of Eq. 5 can be obtained using the superposition of modal response. For example, the longitudinal deflection of the cable can be written as

(23) $$u(s,t) = \sum_{i=1}^{N} q_i(t)\bar{u}_i(s)$$

where $q_i(t)$ is the generalized coordinate for the i_{th} mode. Using orthogonality of the free vibration mode shapes $\bar{u}_i(s)$, $i = 1, 2, 3 \ldots$, the generalized equation of motion reduces to the following differential equations for the generalized coordinates $q_i(t)$, i=1, 2, 3…

(24) $$M_i(\ddot{q}_i + \omega_i^2 q_i) = Q_i \quad i = 1, 2, 3, \ldots$$

with the generalized mass $M_i = \int_0^L \rho(s)\,\bar{u}_i^2(s)ds$; the generalized force $Q_i = \int_0^L f_x(s,t)\cdot\bar{u}_i(s)ds$, the cable mass per unit length $\rho(s)$, and the external force component in the longitudinal direction $f_x(s,t)$. For modeling of the towing cable

(25) $$Q_i = \int_0^L f_x(s,t)\bar{u}_i(s)ds = \int_0^L F_{x\,aero}(s,t)\bar{u}_i(s)ds + \int_0^L f_{x\,tow-body}(s,t)\bar{u}_i(s)ds$$

Presented at 45th European Rotorcraft Forum, Warsaw, Poland, 17-20 September, 2019

$(f_{x\,tow-body}(s,t) = F_{x\,tow-body} \cdot \delta(s))$

where, $\delta(s)$ is the Dirac delta function, $F_{x\,aero}$ is the longitudinal component of aerodynamic force distribution on the cable, and $F_{x\,tow-body}$ is the longitudinal component of concentrated force acting on the tow body. Note that, for Dirac Delta Function, if $a < s_0 < b$, $\int_a^b \delta(s - s_0)ds = 1$ or $\int_a^b g(s)\delta(s - s_0)ds = g(s_0)$. After some substitutions, the generalized force for the i^{th} mode can be obtained as

(26) $$Q_i = \int_0^L f(s,t) \cdot \bar{u}_i(s)ds = \int_0^L F_{cable}(s,t) \cdot \bar{u}_i(s)ds + F_{tow-body} \cdot \bar{u}_i(0)$$

and the generalized mass for the i^{th} mode can be obtained as

(27) $$M_i = \int_0^L \rho(s) \cdot \bar{u}_i^2(s)ds + M_{tip} \cdot \left(\bar{u}_i(0)\right)^2$$

For simulation of the towing cable dynamics, the ODE in Eq. 24 is solved to obtain the generalized coordinate, q_i, for a selected number of mode shapes, N. The cable deflections are then obtained from the summation of the cable mode shapes multiplied by their modal coordinates

(28) $$\mathrm{u}(\mathrm{s},\mathrm{t}) = \sum_{i=1}^N \bar{u}_i(s) \cdot q_i(t)$$

Applying Non-Stretch Constraint to Modal Representation

Recall that the simulation assumes an inextensible cable, which implies

(29) $$\sqrt{\left(\frac{\partial u}{\partial s}\right)^2 + \left(\frac{\partial v}{\partial s}\right)^2 + \left(1 - \frac{\partial w}{\partial s}\right)^2} = 1$$

with the deflections in all three directions, u, v, w, and the curvilinear coordinate along the cable (from towed body to aircraft), s. However, the vector sum of the longitudinal, lateral, and vertical deflections will violate the non-stretch assumption by extending the cable unevenly. Thus, the non-stretch constraint is applied piecewise. The cable is divided into n segments evenly in the s coordinate. For each segment, deflections can be written as

(30) $$\Delta\bar{u}_i = \Delta u_i * \frac{L/n}{\sqrt{\Delta u_i^2 + \Delta v_i^2 + (1-\Delta w)^2}}$$
$$\Delta\bar{v}_i = \Delta v_i * \frac{L/n}{\sqrt{\Delta u_i^2 + \Delta v_i^2 + (1-\Delta w)^2}}$$
$$\Delta\bar{w}_i = \Delta w_i * \frac{L/n}{\sqrt{\Delta u_i^2 + \Delta v_i^2 + (1-\Delta w)^2}}$$

where Δu_i, Δv_i, Δw_i are the local deflections for i^{th} segment before applying non-stretch constraint, and $\Delta\bar{u}_i$, $\Delta\bar{v}_i$, $\Delta\bar{w}_i$ are the local deflections for i^{th} segment after applying non-stretch constraint.

3.4. Combined 3-D deflection shape of the cable

The equations of motion previously described are exclusively for the longitudinal deflection, u. The same approach can be used to derive equations for the lateral and vertical cable deflections. The dynamics of the cable deflections in all directions are considered equivalent to the dynamics in the longitudinal in the sense that all deflections contribute to the moment balance about the cable attachment points. The final result of the cable is obtained as the vector sum of the longitudinal, lateral, and vertical deflections with the non-stretch constraint as described below. Since the governing equation used for free vibration motion is the same for the longitudinal (u), lateral (v), and vertical (w) deflections, the modal frequencies and mode shapes are considered to be the same.

3.5. Normalization of governing equations

Starting from the governing equation

(31) $$\rho\frac{\partial^2 u}{\partial t^2} = \frac{\partial}{\partial s}\left(\|\vec{T}\|\frac{\partial u}{\partial s}\right) + \frac{\partial F_{x\,aero}}{\partial s}$$

and normalizing by cable mass, ρL, the mprmalized governing equation is obtained as

(32) $$\frac{\partial^2 \bar{u}}{\partial t^2} = \frac{\partial}{\partial \bar{s}}\left(\|\bar{T}\|\frac{\partial \bar{u}}{\partial \bar{s}}\right) + \frac{\partial \bar{F}_{x\,aero}}{\partial \bar{s}}$$

Cable deflections, $u, v, and\; w$ and the curvilinear coordinate s are normalized by cable length L, mass and force distributions are normalized by by ρL and force is normalized by ρL^2. The resulting normalized governing equation is of the dimension $1/s^2$. Tables 1 and 2 list the normalized variables and input parameters.

Presented at 45th European Rotorcraft Forum, Warsaw, Poland, 17-20 September, 2019
NAVAIR Public Release 2019-571. Distribution Statement A – "Approved for public release; distribution is unlimited"

Table 1. List of Normalized Variables.

Dimensional	Non-Dimensional
u	$\bar{u} = \frac{u}{L}$
s	$\bar{s} = \frac{s}{L}$
$\|T\|$	$\|\bar{T}\| = \frac{\|T\|}{\rho L^2}$
m	$\bar{m} = \frac{m}{\rho L}$
g	$\bar{g} = \frac{g}{L}$
L	$\bar{L} = \frac{L}{\rho L^2}$
D	$\bar{D} = \frac{D}{\rho L^2}$
$\frac{\partial F_{x\,aero}}{\partial s}$	$\overline{\frac{\partial \bar{F}_{x\,aero}}{\partial \bar{s}}} = \frac{\partial F_{x\,aero}}{\partial s} / \rho L$

Table 2. List of non-dimensional input parameters.

μ	Mass ratio	$\mu \equiv \frac{m_{towed\ body}}{\rho L} = \frac{m_{towed\ body}}{M_{cable}}$
$\bar{d}$	Normalized cable diameter	$\bar{d} = \frac{d}{L}$
$\bar{V}$	Normalized helicopter velocity	$\bar{V} = \frac{V}{L}$
$\bar{\rho}_{air}$	Normalized air density	$\bar{\rho}_{air} = \frac{\rho_{air}}{\rho / L^2}$
$\bar{S}_{ref}$	Normalized towed body reference area	$\bar{S}_{ref} = \frac{S_{ref}}{L^2}$
$\bar{g}$	Normalized gravitational acceleration	$\bar{g} = \frac{g}{L}$
$C_{L_{body}}$, $C_{D_{body}}$	Lift and Drag coefficients of towed body	$C_{L_{body}}$, $C_{D_{body}}$
$C_{D_{cable}}$	Drag coefficient of cable	$C_{D_{cable}}$

4. SIMULATION RESULTS

4.1. Steady State Solution of Cable Dynamics

In the generalized equation of motion of Eq. 24, the aerodynamic forces provide damping to the cable dynamics. In the presence of aerodynamic forces, the dynamic system reaches a steady state characterized by a steady cable deflection and with deflection rates and accelerations approximately zero. Hence, the steady state value of the generalized coordinate, q_i, $i = 1, 2, 3, \ldots$, can be obtained using

(32) $$q_{i\ steady\ state} = \frac{Q_{i\ steady\ state}}{\omega_i^2 M_i}, \ i = 1, 2, 3, \ldots$$

The aerodynamic force distribution over the length of the towing cable depends on the cable shape in steady state. Hence, the steady state solution for the cable dynamics requires an iterative approach. The iterative solution is initiated with the cable initially in vertically straight shape. Aerodynamic forces are then applied to the cable and a new cable shape is calculated. The aerodynamic forces are updated and result in a new cable shape and so on. The iterative process is stopped when the cable shape reaches a solution converged to a specified tolerance.

4.1.1. Example of Iterative Calculation to Obtain Steady State Solution

The parameters for the baseline configuration for this example are listed in Table 3.

Table 3. List of Baseline Configuration Parameters.

Operating (cruise) speed	80 knots @ sea level standard day
Tow body mass	6 lbm
Cable length	300 ft
Cable mass per unit length	0.02 lbm/ft
Cable drag coefficient	0.8

Figure 4 shows the convergence history of 15 iterative calculation steps for obtaining a steady state solution for the baseline case. The solution converges to a steady state cable shape after approximately 10 iterations.

Presented at 45th European Rotorcraft Forum, Warsaw, Poland, 17-20 September, 2019

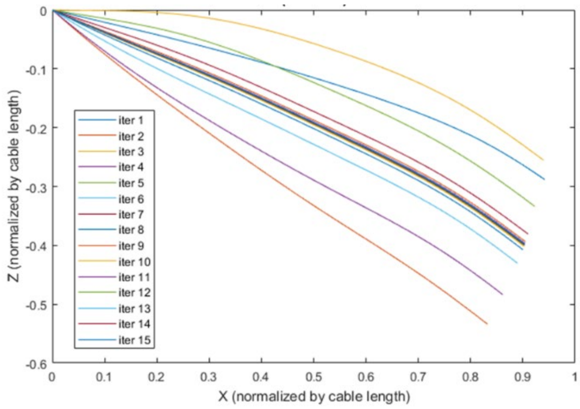

Figure 4. Convergence history of iterative calculation for finding steady state solution.

4.1.2. Comparison of Steady State Solution Using Modal Representation and a Discretized Cable Model

Steady state results from simulations using the modal representation of cable deflection from the present study are compared with similar results from a previously developed discretized cable model[3] in order to confirm that both methods yield similar results and to compare the computational effort for both methods.

Figure 5(a) shows the comparison of steady state results for 300 ft of cable length, 6 lbm of towed body mass, and for different helicopter cruise speeds. Figure 5(b) shows similar results for 100 ft of cable length, 6 lbm of towed body mass, and for different helicopter flight speeds. Figure 5(c) shows results for various towed body masses with 300 ft of cable length and 80 knots of helicopter speed. The comparison of the simulation results from the modal and discretized cable models in Figure 5 shows excellent agreement.

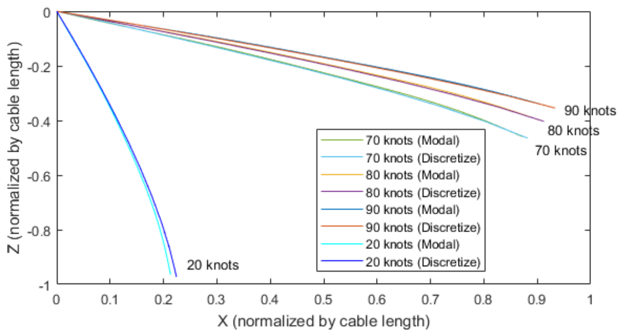

(a) $m_{TB} = 6\ lbm, L = 300\ ft$

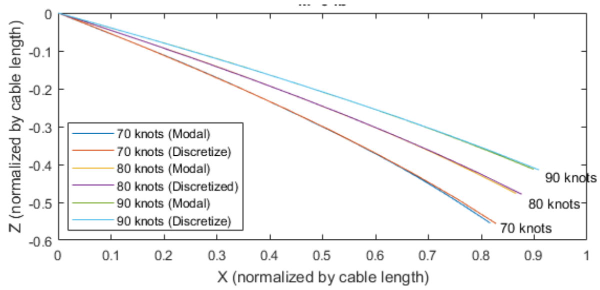

(b) $m_{TB} = 6\ lbm, L = 100\ ft$

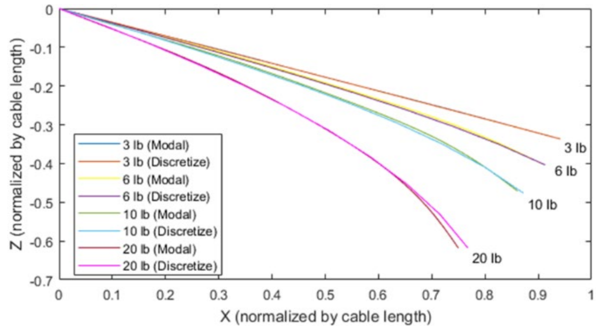

(c) $m_{TB} = varying, L = 300\ ft$

Figure 5. Comparison between steady state solutions from modal representation and discretized model of Ref. 3.

4.2. Cable Deflection during Transient Motion

The transient motion of the towing cable is modeled using a time-varying algorithm. The generalized equation of motion of Eq. 24 is rearranged to get

$$\ddot{q}_i = \frac{Q_i}{M_i} - \omega_i^2 q_i \tag{33}$$

A fourth-order Runge-Kutta method is implemented for the numerical integration of Eq. 33.

4.2.1. Example of Transient Cable Motion – Case A

Figure 6 shows results for transient cable motion (Case A). In this case, the initial cable shape was set as a straight vertical line with zero initial velocity and with the helicopter moving at a constant speed of 80 knots. Note that the towed body is represented as a point mass with aerodynamic lift and drag forces alone. Figure 6(a) illustrates the time history of the cable motion and deflections. Lines are drawn for various time steps of the time-marching simulation. The graph shows the deflections in the vertical (x-z) plane. Figures 6(b) and 6(c) show the time histories of the longitudinal and vertical motions of the towed body, respectively, for Case A.

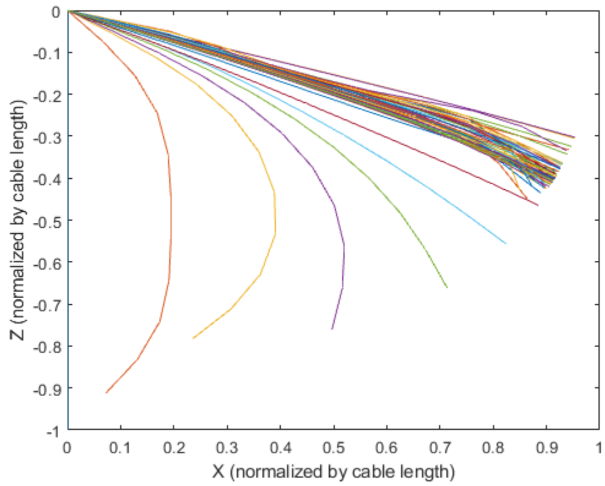

(a) Cable motion (each line a time step)

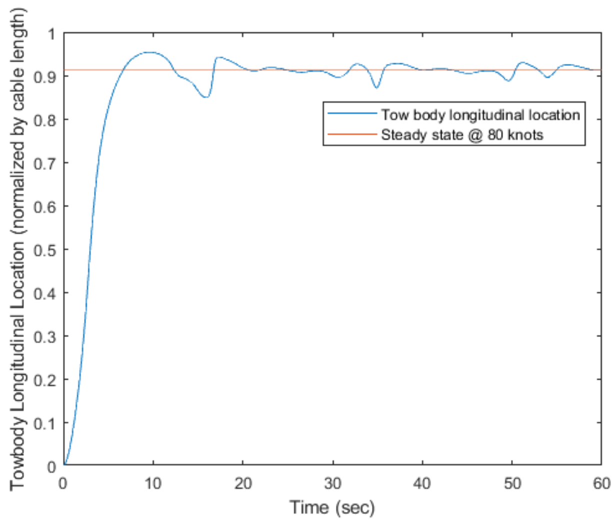

(b) Towed body longitudinal displacement

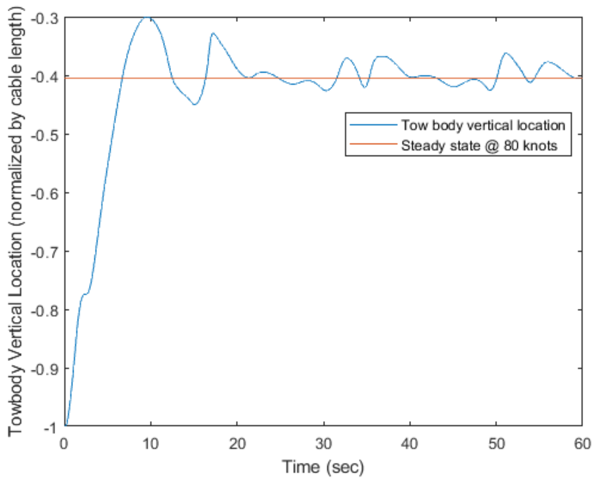

(c) Towed body vertical displacement

Figure 6. Example results of transient motion - Case A.

4.2.2. Example of Transient Cable Motion - Case B

Figure 7 shows results for transient cable motion for Case B where the helicopter and towing cable were initially in steady state at 80 knots cruise speed. The helicopter then decelerates to 70 knots with a maximum deceleration of 0.2g (shown in Fig. 7(b)). Note that the towed body is represented as a point mass with aerodynamic lift and drag forces alone. Figures 7(c) and 7(d) show the histories for the towed body longitudinal and vertical displacements, respectively. The forces on the aircraft towing hook are shown in Fig. 7(e).

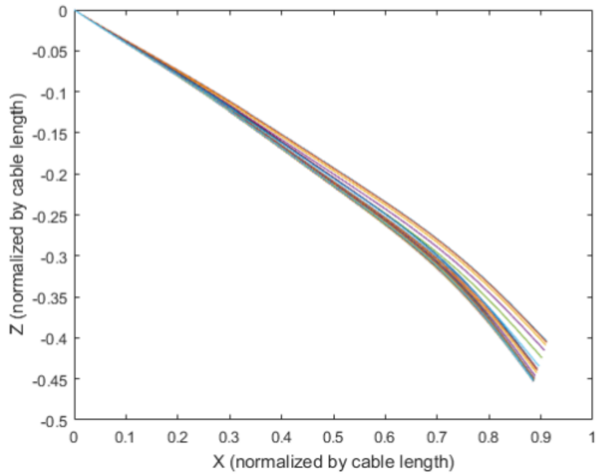

(a) Cable motion (each line a time step)

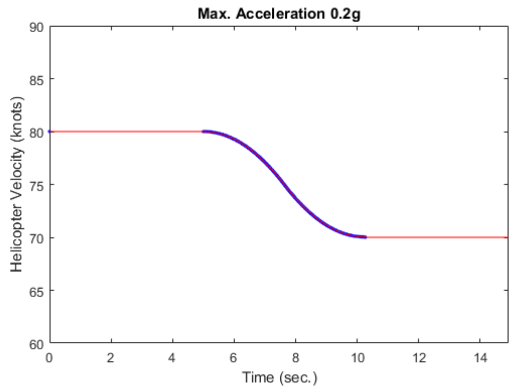

(b) Helicopter airspeed history

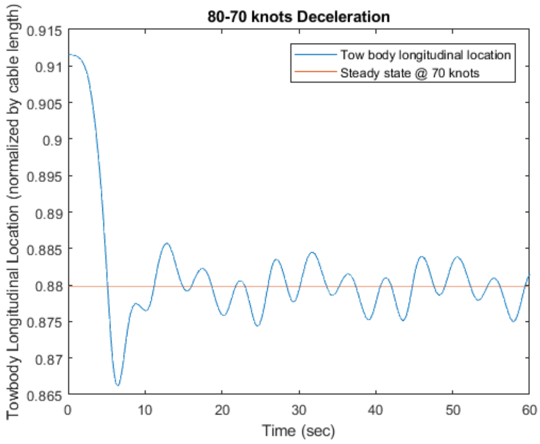

(c) Towed body longitudinal displacement

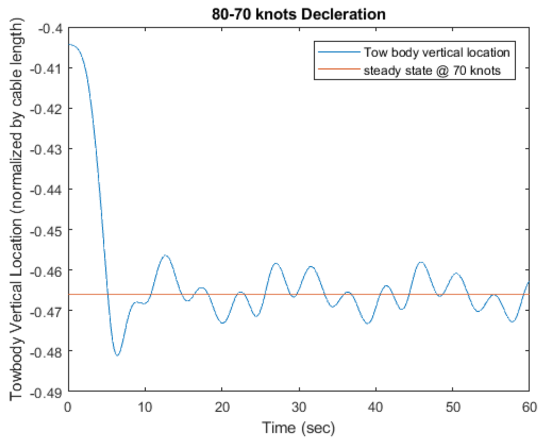

(d) Towed body vertical displacement

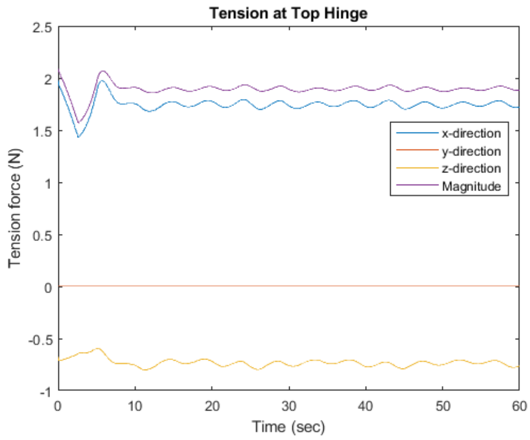

(e) Aircraft hook loads

Figure 7. Example results of transient motion - Case B.

4.2.3. Example of Transient Cable Motion - Case C

Figure 8 shows the results for the transient cable motion for Case C where the helicopter was initially in hover with the cable vertically below the helicopter and in equilibrium. A constant horizontal force of 13.5 lbf was then applied to the towed body. Note that the aerodynamic forces from the free stream were omitted in this case. The only aerodynamics acting on the cable were due to cable and towed body motions. The result converged to the theoretical result from the force balance. Note that the aerodynamic damping in this case was small since the free steam velocity was approximately zero.

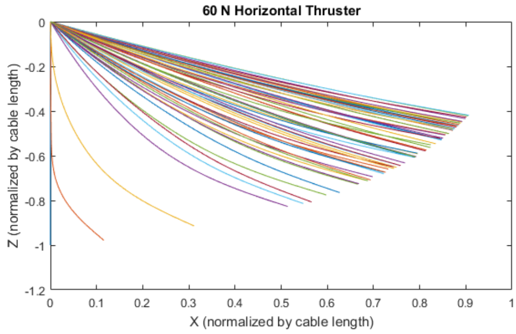

(a) Cable motion (each line a time step)

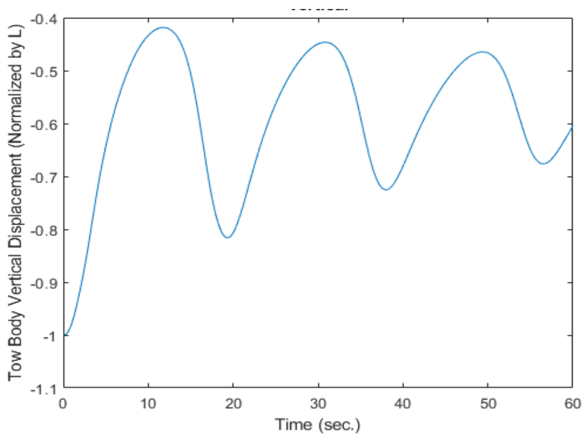

(b) Towed body vertical displacement

Figure 8. Example results of transient motion - Case C.

4.2.4. Example of Transient Cable Motion - Case D

Figure 9(a) shows the transient results for Case D. Initially, the helicopter is at a speed of 80 knots. The helicopter then turns 180 deg with constant speed

Presented at 45th European Rotorcraft Forum, Warsaw, Poland, 17-20 September, 2019
NAVAIR Public Release 2019-571. Distribution Statement A – "Approved for public release; distribution is unlimited"

and an acceleration of 0.5g. Figures 9(b), 9(c), and 9(d) provide the towed body deflection in the longitudinal, lateral and vertical directions in the body-fixed reference frame during the turning maneuver. Figure 9(e) shows the components of the normalized tension force (i.e., normalized by cable weight) at the helicopter towing hook during the turn maneuver.

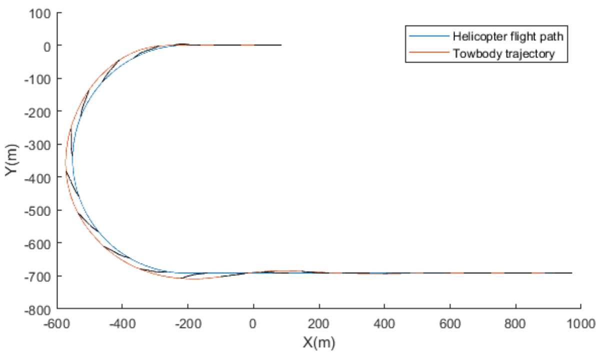

(a) Flight path

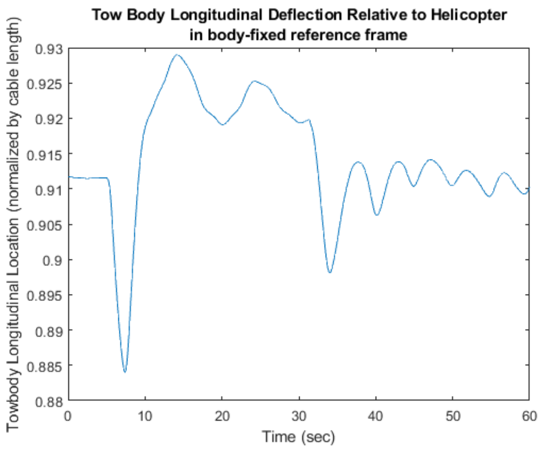

(b) Longitudinal deflection

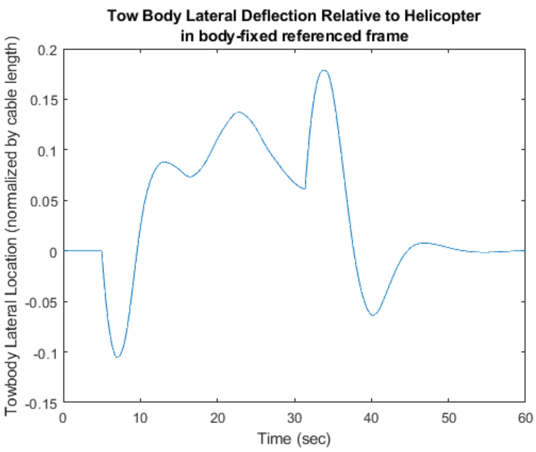

(c) Lateral deflection

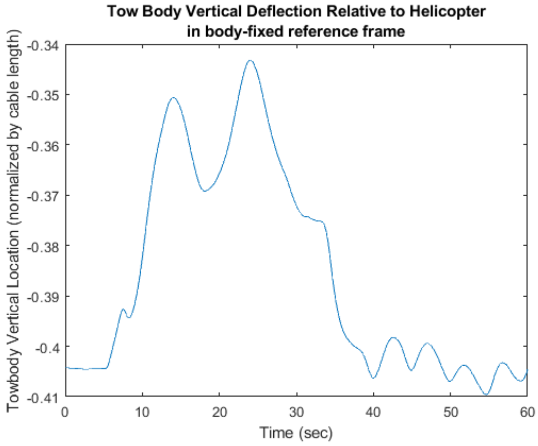

(d) Vertical deflection

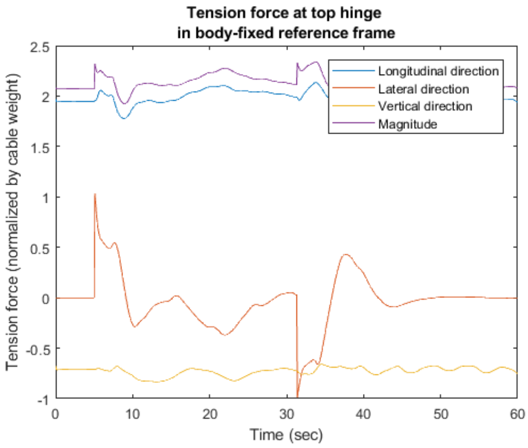

(e) Towing hook loads

Figure 9. Transient results for Case D (Helicopter in a steady turn at 80 knots speed).

4.3. Computational Efficiency of the Cable Model

In order to improve the computational efficiency of the cable model, polynomial curve fitting was implemented to the mode shapes and the aerodynamic force distribution. Since derivative and integral evaluation of polynomials is linear mapping, the entire simulation process was converted to be based on matrix calculations, thus improving the computational efficiency. As a result, in order to simulate 60 seconds of cable motion, the time consumed was around 40 seconds for a single-core computer with 48GB of available memory (RAM). It was noticed, albeit not investigated in detail, that the amount of memory available affects the computational time.

4.4. Parametric Study of Towing Simulation Using New Cable Model

Parametric studies were performed to better understand the towing system dynamics in response to changes in design parameters and the use of the new cable model. The main design parameters considered were the cable length, the mass ratio (i.e., between cable and towed body), and the towing cable diameter.

In order to compare the system response for variations of design parameters, the root mean square

(RMS) value for the oscillation was calculated for a duration equivalent to two pendulum periods after the helicopter maneuver ends, as illustrated in Fig. 10.

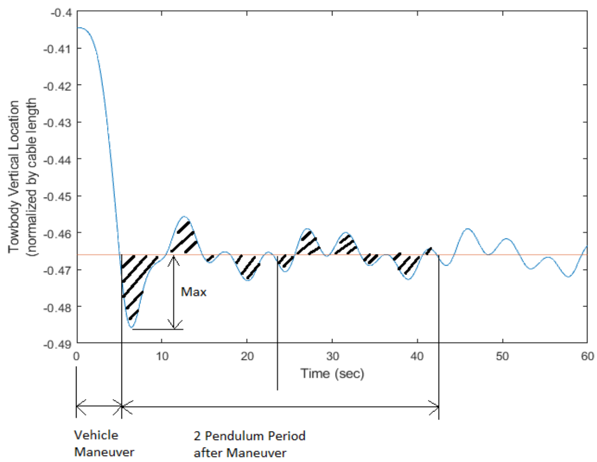

Figure 10. Simulation duration used for determination of root mean square (RMS).

For a flexible pendulum, the 1st mode frequency (pendulum frequency) depends on the cable

length and the mass ratio, μ, defined as

$$\mu = \frac{Tow\ Body\ Mass}{Cable\ Mass}$$

Figure 11 shows the value of the 1st mode frequency for different cable lengths and mass ratios. It shows that, for a given cable length, when the mass ratio is small, the 1st mode frequency is somewhat higher than the theoretical rigid pendulum frequency. As the mass ratio approaches infinity, the 1st mode frequency approaches the theoretical rigid pendulum frequency.

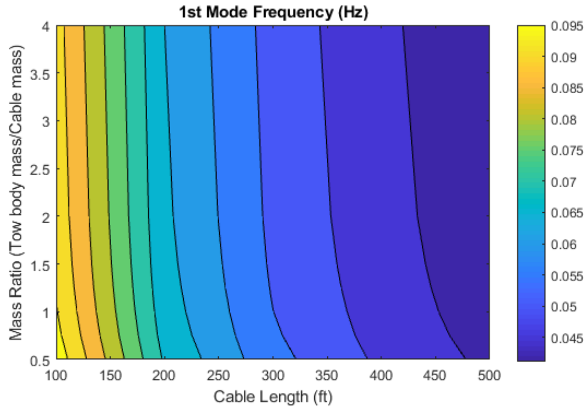

Figure 11. First cable mode frequency, pendulum frequency, as a function of cable length and mass ratio.

4.4.1. Mass Ratio Variation

The effect of variation of the mass ratio is illustrated for the towed body vertical deflection during the 80 to 70 knot deceleration maneuver and for four different configurations (see Fig. 12). The cable length and the cable diameter were kept constant and the mass ratio was varied. For towing systems with a higher mass ratio, pendulum motion tends to dominate the system response. As the mass ratio decreases, flexible mode motion is blended into pendulum motion and eventually comes to dominate the towing system response. As shown in Table 4, a higher mass ratio also leads to a higher oscillation RMS and maximum amplitude.

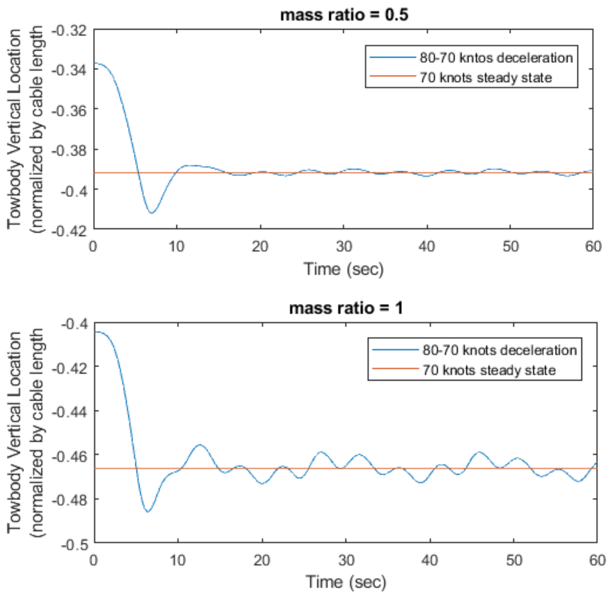

Presented at 45th European Rotorcraft Forum, Warsaw, Poland, 17-20 September, 2019

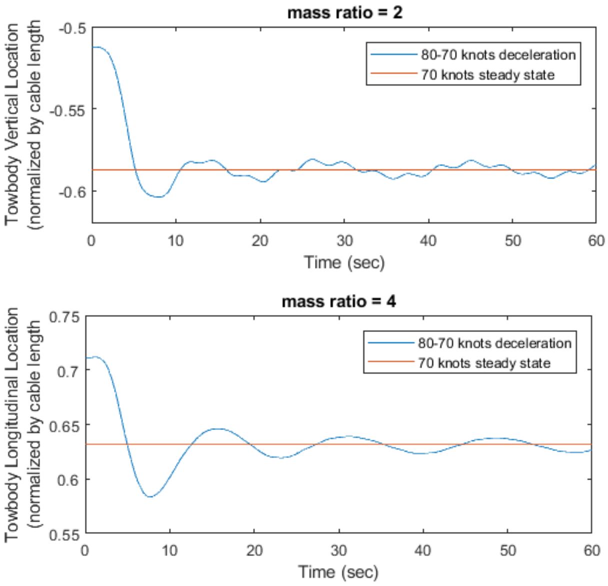

Figure 12. Towed body vertical deflection during the 80 knot to 70 knot deceleration for different mass ratios, μ.

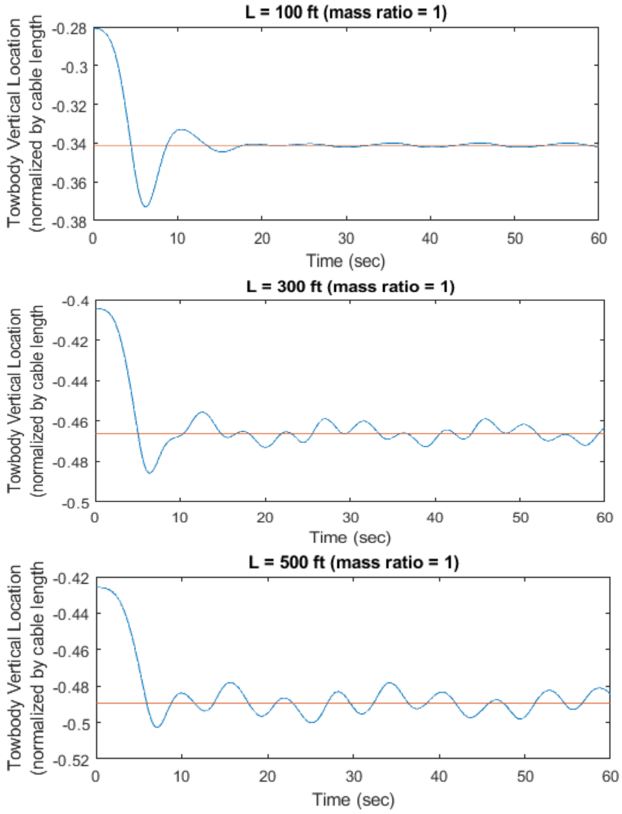

Figure 13. Tow body vertical deflection during 80 knot to 70 knot deceleration with different cable lengths, L.

Table 4. Oscillation RMS and maximum amplitude after 80 knot to 70 knot deceleration for different mass ratios.

Mass Ratio	Oscillation RMS (normalized by cable length)	Oscillation Max (normalized by cable length)
0.5	0.005447	0.02264
1	0.007316	0.02610
2	0.009947	0.02795
4	0.01831	0.05430

4.4.2. Cable Length Variation

Studies were conducted with a constant mass ratio and with varying cable length. Figure 13 shows the towed body vertical deflection during the 80 knot to 70 knot deceleration maneuver. A short cable length leads to a more dominant pendulum motion, smaller oscillation RMS, but larger overshoot.

Table 5 shows the RMS and maximum amplitude for oscillation for the maneuver for different cable lengths.

Table 5. Oscillation RMS and Max value after the 80 knot to 70 knot deceleration maneuver for different cable lengths.

Length (ft.)	Oscillation RMS (normalized by cable length)	Oscillation Max (normalized by cable length)
100	0.01050	0.03409
200	0.008055	0.02768
300	0.007316	0.02610
400	0.007806	0.02599
500	0.008709	0.02595

4.4.3. Combination of Mass Ratio and Cable Length variations

Figure 14 shows how different combinations of mass ratio and cable length affect the oscillation RMS and maximum amplitude for the 80 knot to 70 knot deceleration maneuver. In the oscillation RMS contour (see Fig. 14a)), it can be seen that, for a given small mass ratio, an optimal cable length may be found in order to minimize the oscillation RMS.

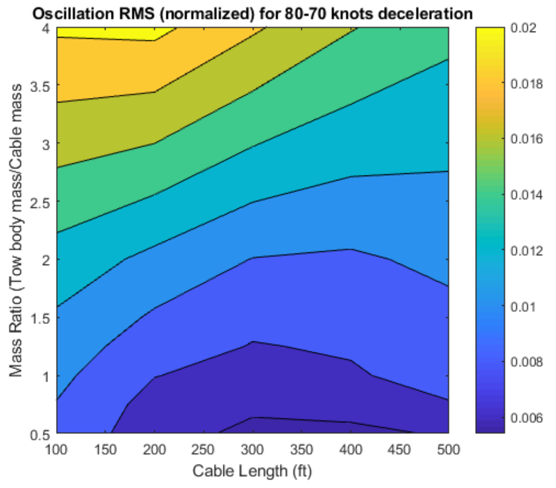

(a) Oscillation RMS (normalized)

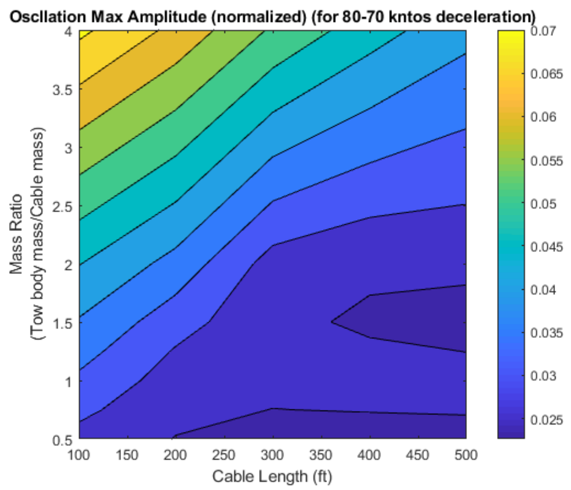

(b) Maximum. amplitude (normalized)

Figure 14. Contours for oscillation RMS and maximum amplitude for 80 knot to 70 knot deceleration maneuver for different cable mass ratios and cable lengths.

4.4.4. Cable Diameter Variations

Figure 15 illustrates the towed body vertical deflection during the 80 knot to 70 knot deceleration maneuver for configurations with different cable diameters and constant cable mass ratio. A constant cable material density is assumed. Thus, for a larger cable diameter, the towed body mass is increased to maintain constant mass ratio. The results show that a smaller cable diameter leads to a more dominant pendulum motion and less overall oscillation amplitude. It is seen that smaller cable diameter leads to more dominated pendulum motion and less overall oscillation amplitude.

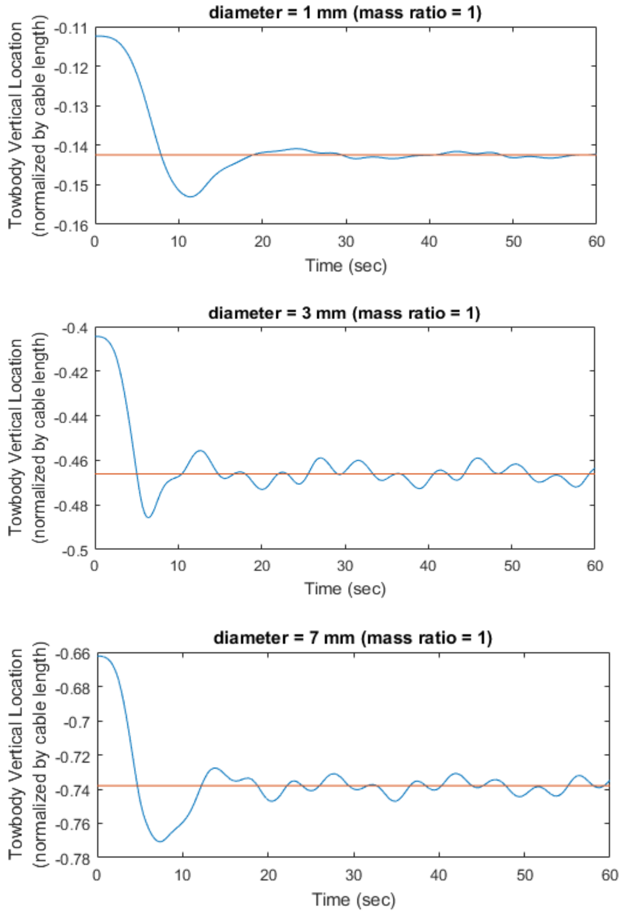

Figure 15.Towed body vertical deflection during the 80 knot to 70 knot deceleration maneuver for different cable diameters and constant mass ratio.

4.4.5. Cable Material Density Variations

It was observed that with a fixed value of the cable mass per unit length (ρ), increasing the cable diameter (i.e., a decrease in cable material density) beyond a critical value resulted in random cable motion and simulation divergence. Table 6 lists the critical cable diameters before the dynamics of the towing system diverge for different cable lengths and mass ratios.

Table 6. The critical cable diameter (mm) before the system divergence with constant mass per unit length.

Cable Length	Mass Ratio			
	0.5	1	2	4
L=200 ft	13	13	12	15
L=300 ft	8	8	8	10
L=400 ft	6	6	7	8

For a given baseline cable mass per unit length, the results above suggest cable material density limits, which are listed in Table 7. The result suggests that, for the baseline configuration, any cable made with metal may be acceptable, but the ultra-low weight rope may not be suitable for the application.

Table 7. The critical cable material density (kg/m^3) before the system divergence with baseline cable mass per length.

Cable Length	Mass Ratio			
	0.5	1	2	4
L=200 ft	224	224	263	168
L=300 ft	468	592	592	379
L=400 ft	1053	1053	773	692

5. CONCLUDING REMARKS

A simulation model of towing system for rotorcraft is developed using the modal representation approach. The free vibration mode shapes of a hanging cable with end mass, as previously shown in the literature, are found to be in the form of Bessel functions. Aerodynamic forces on both cable and towed body are treated as external forces, and are included in the modal form of the equations using the generalized force formulation. The developed model of the cable/towed body system in modal form is numerically integrated to study the effect of vehicle maneuvers on unsteady motion of the cable/tow body system. A comparison of the steady state results from the present model with those from a previously developed discretized model show very good agreement between the two models. The computing time for a one minute of transient simulation with the new model using a single core machine with 48GB RAM is seen to be roughly 40 sec., implying that the modal form of the cable/tow body system model developed in the present study can be used in real time simulations.

Simulations are carried out using the modal form of the equations of motion of the cable/tow body system with the helicopter executing constant acceleration/deceleration maneuvers or a turn maneuver. The resulting transient cable deflections and towed body motion are noted to be qualitatively correct. Simulations are performed to understand the impact of variations of cable/tow body system parameters, such as, cable and towed body mass ratio, cable length, cable diameter, cable material density, on the transient cable deflections and towed body unsteady motion. Based on the results presented, the following general conclusions are drawn:

1. A smaller cable diameter usually tends to contribute to a more stable towing system.

2. A smaller mass ratio results in lower RMS values of cable/tow body oscillations, albeit with larger steady state deflections of the cable.

3. For smaller values of mass ratios, there may exist an optimal cable length that can result in minimal RMS oscillations of cable/tow body system.

4. With a fixed value of cable mass per unit length, increasing the cable diameter (i.e., a decrease in cable material density) beyond a critical value can lead to simulation divergence.

While the modal form of the cable/tow body system model developed in this study is seen to be computationally efficient, further work is needed in order to address the following enhancements.

1. The current study uses a simplified aerodynamic model for the towed body, mostly represented as lift and drag forces using a point mass approximation. Further studies are needed with a detailed aerodynamic model of the towed body that includes both aerodynamic forces and moments.

2. The current study assumes quasi-steady aerodynamics for the towing cable. Future studies need to consider unsteady aerodynamics of the cable in order to fully capture the coupling between the vortex shedding from the cable and its oscillations.

3. While the current model is seen to produce results similar to a previously developed (computationally expensive) discretized model of the cable/tow body system, future

Presented at 45th European Rotorcraft Forum, Warsaw, Poland, 17-20 September, 2019

work must include correlations with experimental data.

Author contact:

J.V.R. Prasad jvr.prasad@ae.gatech.edu
Zhenhao Jing jzh@gatech.edu
L.N. Sankar Lakshmi.sankar@ae.gatech.edu
C.He chengjian.he@flightlab.com
J. Goericke jan.goericke@flightlab.com

6. ACKNOWLEDGEMENT

This project was funded by award from the Naval Air Systems Command (NAVAIR) as a STTR, contract number N68335-16-C-0269.

7. REFERENCES

[1] He, C., Zhao, J. and Jan G.,“ Multi-Body and Unsteady Rotorcraft/Slung Load Modeling and Simulation,” 32nd European Rotorcraft Forum, Sept. 2006, Mastricht, The Netherlands.

[2] Xin, H. and He, C., “A High Fidelity Simulation Model for Comprehensive Analysis of Rotorcraft Towing Operations,” Proceedings of 59th AHS Annual Forum, Phoenix, Arizona, May 6-8, 2003.

[3] Liu, Y. and Prasad, J.V.R., “Dynamic simulation of a Towing System,” Internal Project Report, School of Aerospace Engineering, Georgia Institute of Technology, 2015.

[4] Leijonhufvud, M. C. and Lindberg, A., “Dynamic simulation of a towed decoy system,” 26th International Congress of the Aeronautical Sciences, 2008.

[5] Sujith, I. and Hodges, D. H., “ Exact Solution for the Free Vibration of a Hanging Cord with a Tip Mass,” Journal of Sound and Vibration, 359-361, 1995.

[6] Barnes, B. J., “Wind Tunnel Measurement of Airborne Towed Cable Drag Coefficients,” NSAF Report, p. 41, 1971.